# Universal Critical Behavior of Percolation in Orientationally Ordered Janus Particles and Other Anisotropic Systems

Hao Hu*
*School of Physics and Optoelectronic Engineering, Anhui University, Hefei 230601, China*

Robert M. Ziff
*Center for the Study of Complex Systems and Department of Chemical Engineering, University of Michigan, Ann Arbor, Michigan 48109-2800, USA*

Youjin Deng
*Department of Modern Physics, University of Science and Technology of China, Hefei 230026, China and MinJiang Collaborative Center for Theoretical Physics, College of Physics and Electronic Information Engineering, Minjiang University, Fuzhou 350108, China*

(Received 13 June 2022; accepted 7 December 2022; published 29 December 2022)

We combine percolation theory and Monte Carlo simulation to study in two dimensions the connectivity of an equilibrium lattice model of interacting Janus disks which self-assemble into an orientationally ordered stripe phase at low temperature. As the patch size is increased or the temperature is lowered, clusters of patch-connected disks grow, and a percolating cluster emerges at a threshold. In the stripe phase, the critical clusters extend longer in the direction parallel to the stripes than in the perpendicular direction, and percolation is thus anisotropic. It is found that the critical behavior of percolation in the Janus system is consistent with that of standard isotropic percolation, when an appropriate spatial rescaling is made. The rescaling procedure can be applied to understand other anisotropic systems, such as the percolation of aligned rigid rods and of the $q$-state Potts model with anisotropic interactions.

DOI: 10.1103/PhysRevLett.129.278002

The novelty of Janus particles [1], which have two surface areas of different properties, was appreciated very early in the field of soft matter [2]. Nowadays the particles can be synthesized by various methods and are used as surfactants, micromotors, displays, catalysts, biosensors, etc. [3–6]. The possibilities offered by Janus particles mainly depend on the fact that heterogeneous surfaces lead to anisotropic interactions. Harnessing the unique interactions, unconventional self-assembled structures can be made, such as gases of micelles [7,8], entropy stabilized open crystals [9,10], and crystals of orientational order [7,11–25]. However, in orientationally ordered Janus systems, long-range connectivity behavior, which is important to understand transport [26], mechanical [27], dynamical [28,29], and other properties [30,31], remains largely unexplored [11,19,32].

Recently it was found that, in the orientationally ordered nematic phase of slender nanoparticles, the coupling between the particle density and the orientational order gives rise to interesting nonmonotonic behavior of the percolation threshold as a function of the density [33,34]. Percolation deals with long-range connectivity and is one of the most applied models in statistical physics [30,31,35,36]. At the percolation threshold, a system-spanning connected cluster first appears, and there exist various universal properties, e.g., critical exponents, dimensionless quantities, correlation and scaling functions [37]. For percolation in anisotropic systems, while some results have been obtained on thresholds and critical exponents [29,33,34,38–45], other universal critical properties, such as the continuous change of dimensionless wrapping probabilities of aligned rigid rods [43–45], are not well understood.

For most systems of Janus particles, positional and rotational motions are coupled, which leads to complex phase behavior. However, for close-packed crystals of Janus particles, positional vibrations are much less important. Thus close-packed Janus systems provide a platform where one can tune controlling parameters, e.g., the temperature or pressure, to explore orientaional order driven by rotational fluctuations [18–24,46,47]. In this Letter, by exploring anisotropic interacting close-packed Janus disks in two dimensions (2D), we ask how thermal rotational fluctuations affect universal critical behavior of anisotropic percolation in crystal phases of orientational orders, and how the results can be generalized to understand percolation in other anisotropic systems.

We use a simple model of Janus disks on the triangular lattice, where particles interact with the Kern-Frenkel potential [48]. Combining percolation theory and Monte Carlo

 

(MC) simulation, we find that, in the orientationally ordered stripe phase [23], though critical exponents are consistent with standard isotropic percolation, universal values of dimensionless quantities (e.g., Binder-like ratios and wrapping probabilities [49]) change continuously along the percolation line. Using theoretical results for wrapping probabilities of standard percolation in 2D [50–53], we find an effective aspect ratio $\rho_e$ to perform a spatial rescaling and relate quantitatively universal critical behavior of percolation in the stripe phase to that of standard percolation. Thus the mechanism underlying the continuous variations of dimensionless quantities is that anisotropic interactions in the stripe phase cause connectivity correlations to be anisotropic, but the behavior can be captured by standard percolation. We then show that the mechanism can also explain anisotropic percolation behavior in other systems, such as systems of particles with anisotropic shapes (e.g., aligned rigid rods [43–45]), and systems of anisotropic bond-placing rules. For the latter systems, by studying anisotropic bond percolation [38,39] on the triangular lattice, we demonstrate by the isoradial-graph method [41,42] that a more general relation between anisotropic percolation and standard percolation requires an effective shear transformation involving both $\rho_e$ and an effective boundary twist $t_e$. In terms of conformal invariance and universality, statistical models on isoradial graphs have nice properties [54], which we further use to derive $\rho_e$ and $t_e$ for understanding universal critical behavior of percolation in the anisotropic $q$-state Potts models [53]. The results may help design materials with tunable anisotropic connectivity-related properties such as ferroelectricity [29], conductivity [55,56], and photovoltaics [57].

The model system consists of close-packed Janus disks with monodisperse patch sizes in 2D. Rhombus-shaped $L \times L$ triangular lattices with periodic boundary conditions are used, and each lattice site is occupied by a disk with diameter 1. To allow only rotational motions, the center of each disk is fixed at a lattice site. As shown at the top left of Fig. 1, the dark sector represents a patch on the disk which spans an angle of $2\theta$. The half-patch angle $\theta$ (i.e., the Janus balance [58]) characterizes the patch size. The Janus disks interact with a Kern-Frenkel potential [48]: two nearest-neighbor disks contribute an energy $-\epsilon$ if the two patches on them cover the same edge and touch each other; otherwise, they contribute a zero energy. When studying percolation, two disks are regarded as connected when they interact with an energy $-\epsilon$. The unit of temperature $T$ is $\epsilon/k_B$, where $k_B$ is the Boltzmann constant.

Figure 1 shows the phase diagram in the $T-\theta$ plane. Previously it was found that, for $1/3 < \theta/\pi \leq 1/2$, there is a continuous thermodynamic phase transition from a high-$T$ disordered phase to a low-$T$ orientationally ordered stripe phase [23]. For close-packed Janus particles in 2D continuum space, preliminary results showed that this thermodynamic phase transition is still continuous [17]. Since at $T=\infty$ the percolation threshold is $\theta_p/\pi = 0.627\,765\,41(3)$ [32], to explore connectivity at finite $T$,

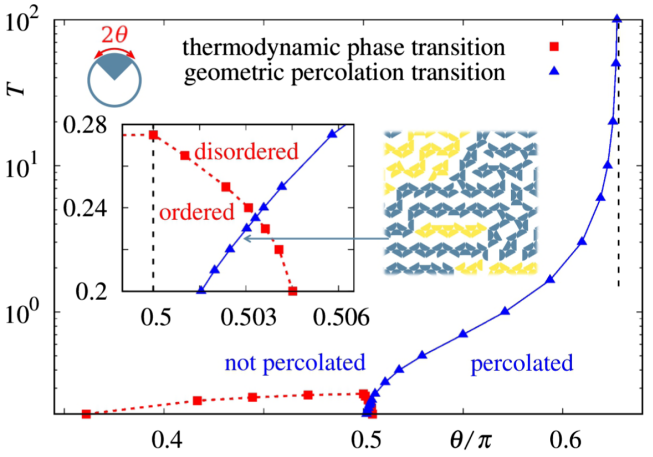


FIG. 1. Phase diagram of close-packed Janus disks in 2D. The system is ordered below the phase-transition line with squares, and it is percolated to the right side of the percolation-transition line with triangles. According to whether the system is ordered or percolated, the diagram is divided into four regions: an ordered and (not) percolated region, and a disordered and (not) percolated region. Inset: enlargement near $\theta/\pi = 0.503$, as well as a snapshot of an ordered and percolated configuration, with the largest cluster being dark blue. Vertical dashed lines indicate the position of $\theta/\pi = 1/2$ and the infinite-temperature percolation threshold $\theta_p/\pi \simeq 0.628$ [32]. Lines going through data points are added to guide the eye, and the error bars are smaller than or comparable with the symbols.

we need first understand thermodynamic behavior for $\theta/\pi > 1/2$. We performed extensive simulation using the Metropolis algorithm, where in a MC sweep the disks are sequentially visited and independently proposed to rotate by a random angle in the range $[-\pi, \pi)$. An orientational order parameter based on the structure factor and the associated Binder ratio defined in Ref. [23] were sampled [53]. We find that the continuous phase transition from the disordered phase to the stripe phase also exists for $\theta/\pi > 1/2$, and determine the phase transition line [53] as plotted in Fig. 1.

To explore connectivity of the Janus disks, we combine the critical polynomial method [59–64] with MC simulation. In the probabilistic geometric interpretation [62], for standard percolation in 2D, the critical polynomial is defined as $P_B \equiv R_2 - R_0$, where $R_2$ is the probability that there exists a cross-wrapping cluster and $R_0$ is the probability of no wrapping. The root of $P_B = 0$ gives the percolation threshold when $L \to \infty$. The critical polynomial has been demonstrated to be very powerful in determining percolation thresholds in 2D [32,64,65]. Wrapping probabilities were sampled in our simulation. Near the whole percolation line, curves of $P_B(\theta, L)$ cross, and the crossing points converge quickly to $P_B = 0$. The fact that $P_B(\theta_p, L \to \infty) = 0$ suggests that the percolation transition belongs to the universality class of standard percolation, since this limit is not true for other models such

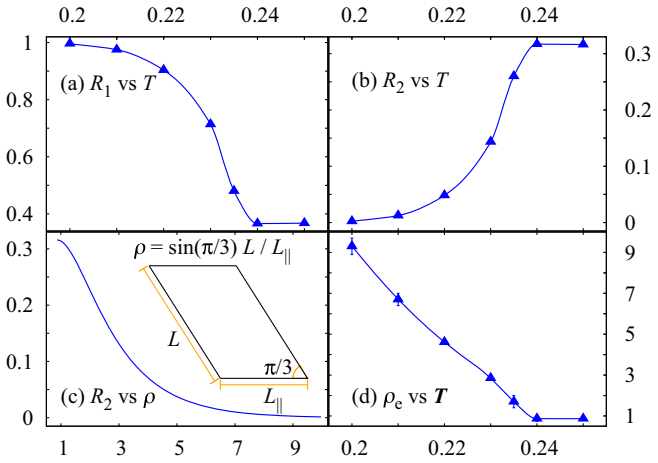


FIG. 2. Critical wrapping probabilities along the percolation line [i.e., solid curve with triangular points $T(\theta)$ in Fig. 1] of the Janus system. (a) Probability of wrapping in only one direction $R_1$ vs $T$. (b) Wrapping probability $R_2$ vs $T$. (c) Theoretical curve of $R_2$ vs the aspect ratio $\rho$ for standard percolation on parallelogram-shaped periodic lattices. (d) The effective aspect ratio $\rho_e$ vs $T$ for the Janus system.

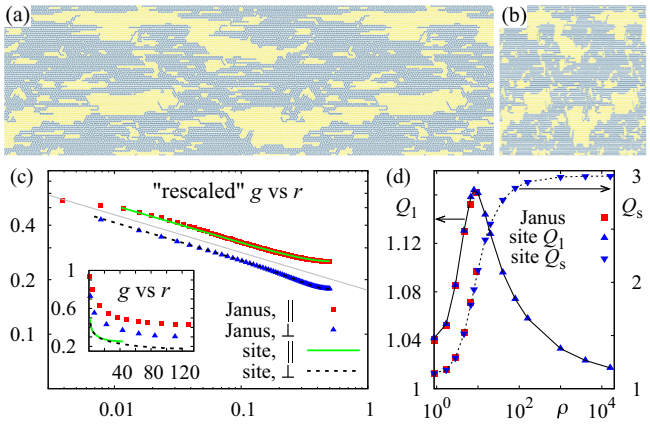


FIG. 3. Relations between percolation in the stripe phase of the Janus system and standard site percolation on the triangular lattice. (a) A snapshot of the Janus system at $\theta_p/\pi = 0.503\,027(2)$, with $T = 0.23$ and $L = 256$, which is ordered in the parallel (horizontal) direction. The dark blue region represents the largest wrapping cluster, with its holes being light yellow. (b) Isotropic configuration after rescaling the parallel direction by $\sqrt{3}/(2\rho_e)$, with $\rho_e \simeq 2.85$. (c) Collapse of critical correlations of the Janus system and those of site percolation on the triangular lattice with size $L_{\parallel} \times L = 88 \times 290$. The light gray line has a slope $-5/24$ from percolation universality. (d) Collapse of critical ratios $Q_1$ and $Q_s$ [78,79] of the Janus system and those of site percolation with $\rho = \rho_e$.

as the $q$-state Potts model [66]. We perform finite-size scaling analysis and find that critical exponents indeed take values for standard percolation [53]. The estimated percolation thresholds at different $T$ are shown by blue triangles in Fig. 1. It is seen that, as $T$ drops, the value of $\theta_p$ decreases and approaches $\theta = \pi/2$ in the low-$T$ limit. Thus, the orientationally ordered stripe phase is not guaranteed to be percolated.

From the theory of critical phenomena, scale invariance at the percolation threshold is related to the fact that many dimensionless quantities are independent of the system size, if finite-size corrections are neglected. Critical values of dimensionless quantities are "universal" [37] in the sense that a quantity holds the same value for different lattices, short-range interactions, etc. For wrapping probabilities, along the percolation line we find that, in the disordered phase, they indeed take the same values as those for standard percolation for systems of the same shape [51,67]. However, in the stripe phase ($T < 0.24$), we find that they change continuously as shown in Figs. 2(a) and 2(b). This implies that the orientational order affects "universal" critical properties.

It has been known that "universal" values of critical dimensionless quantities still depend on factors such as the system shape and boundary conditions [51,52,67–69], anisotropy of couplings [70–77], and statistical ensembles [49]. Thus we are interested in whether or how our results above could be connected with existing results for standard percolation. From the configurations near $\theta_p$ in the stripe phase, it is seen that clusters are longer in the parallel direction than in the perpendicular direction, as exemplified in Fig. 3(a). After rescaling the parallel direction by an appropriate factor, the configuration becomes isotropic, as shown in Fig. 3(b). The rescaling transforms an anisotropic system with size $L \times L$ to an effective isotropic system with size $L_{\parallel} \times L$ where $L_{\parallel} < L$. This leads us to hypothesize that anisotropic percolation of the $L \times L$ rhombus-shaped Janus system is related to standard percolation on a parallelogram-shaped triangular lattice of size $L_{\parallel} \times L$ as depicted in the inset of Fig. 2(c), i.e., the Janus system has an effective aspect ratio $\rho_e = \rho \equiv L_{\perp}/L_{\parallel} = \sin(\pi/3)L/L_{\parallel}$, and the rescaling factor is $L_{\parallel}/L = \sqrt{3}/(2\rho_e)$.

For standard percolation in 2D, values of critical wrapping probabilities depend only on $\rho$ and the boundary twist $t$ (being $\rho/\sqrt{3}$ for the parallelogram-shaped periodic triangular lattice), and their exact expressions are available [50–53], as illustrated for $R_2$ in Fig. 2(c). Thus one can compare numerical values of critical wrapping probabilities with the theoretical values to get the $\rho_e$ value. In this way, we get the dependence of $\rho_e$ on $T$ for the Janus system, as shown in Fig. 2(d). While $\rho_e$ equals $\sqrt{3}/2$ in the disordered phase, it monotonically increases as $T$ drops in the stripe phase, and should approach infinity in the low-$T$ limit.

With the obtained $\rho_e$, we test our above hypothesis as follows. Beside the direct view from Fig. 3(a) to Fig. 3(b), we calculate the correlations $g(r)$ (probabilities of two particles at a distance $r$ in the same cluster) in both the parallel and perpendicular directions at $\theta_p$. As shown in Fig. 3(c) for $T = 0.23$, the correlations of the Janus system can be

collapsed into those of standard site percolation by (1) defining the $x$ axis to be $r_\parallel/L_\parallel = r/L$ and $r_\perp/L_\perp = 2r/\sqrt{3}L$, thus $\tilde{g}_\parallel(r/L) = g_\parallel(r)$ and $\tilde{g}_\perp(2r/\sqrt{3}L) = g_\perp(r)$, and (2) multiplying $\tilde{g}$ of the Janus system by a nonuniversal constant (being 0.588 for $T = 0.23$) [53]. Further, we compare critical values of two dimensionless ratios at $\rho = \rho_e$. They are defined as [78,79] $Q_1 = \langle C_1^2\rangle/\langle C_1\rangle^2$, $Q_s = \langle 3S_2^2 - 2S_4\rangle/\langle S_2\rangle^2$, where $C_1$ ($C_i$ for $i \neq 1$) is the size of the largest cluster (other clusters) and $S_l = \sum_i C_i^l$ is the $l$th moment of cluster sizes. It can be seen from Fig. 3(d) that critical values of the two ratios for the Janus system are consistent with those of standard site percolation. Thus the Janus system is quantitatively related to standard percolation through $\rho_e$.

While the anisotropy arises from the emergent orientational order in the stripe phase, it can also come from anisotropic constituent particles or anisotropic bond-placing rules. For the former, we consider aligned rigid rods of various sizes $k$ (also called $k$ mers as a rod occupies $k$ consecutive sites) on periodic $L \times L$ square lattices. In simulation, the system is treated as a random sequential adsorption. By comparing critical values of $R_2$ with the theoretical curve of $R_2$ for standard percolation on rectangular-shaped square lattices ($t = 0$) [50–53], we extract the dependence of $\rho_e$ on $k$, as plotted in Fig. 4(a), which suggests $\rho_e \simeq 0.4k$ for large $k$. The critical values of $Q_1$ and $Q_s$ for the aligned rigid rods are also found to match those for site percolation on square lattices of size $(\rho_e L) \times L$, as plotted in Fig. S11(b) of the Supplemental Material [53]. These explain the continuously varying dimensionless quantities found for aligned rigid rods in Refs. [43–45].

We then consider bond percolation with anisotropic bond-placing rules. For the triangular lattice [Fig. 4(b)], three edges of a triangle are occupied with different probabilities $p_0$, $p_1$, and $p_2$, and the critical probabilities satisfy $p_0 + p_1 + p_2 - p_0p_1p_2 = 1$ [38,39]. Recently the method of isoradial graphs [41,42,54] was developed to prove the equivalence of critical exponents between anisotropic and isotropic systems, but it has not been applied to give values of dimensionless quantities. We expect that, with a shear transformation described by $\rho_e$ and an effective

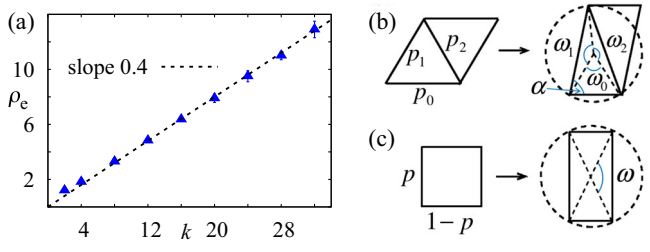


FIG. 4. (a) $\rho_e$ vs $k$ for percolation of aligned rigid rods. (b) and (c) Sketch of the isoradial mapping for anisotropic bond percolation on triangular and square lattices.

boundary twist $t_e$, a critical dimensionless quantity takes the same value on isoradial graphs. After the isoradial mapping, the length of each edge is adjusted to compensate for its weight to make the system conformally invariant in the scaling limit [54], and the angles are determined by the Kenyon-Grimmett-Manolescu formula [41,42] as $\omega_i = 3\arctan[\sqrt{3}(1-p_i)/(1+p_i)]$, $i = 0, 1, 2$, as illustrated in Fig. 4(b) where the rhombus on the left-hand side transforms to a parallelogram with $\alpha = \omega_2/2$. Thus, for the triangular lattice we derive that the isoradial graph has $\rho_e = \sin(\omega_2/2)\sin(\omega_1/2)/\sin(\omega_0/2)$ and $t_e = \cos(\omega_2/2)\sin(\omega_1/2)/\sin(\omega_0/2)$. For the square lattice, the isoradial mapping at criticality is sketched in Fig. 4(c), and we derive $t_e = 0$ and $\rho_e = \tan(\omega/2)$, with $\omega = 3\arctan[\sqrt{3}(1-p)/(1+p)]$. We have numerically verified that wrapping probabilities of anisotropic bond percolation on the triangular and square lattices are equal to theoretical values of standard percolation with the above $\rho_e$ and $t_e$ [53].

It was shown recently that an effective shear transformation also relates the anisotropic Ising model on a square to the isotropic Ising model on a parallelogram [75–77]. In the $q$-state Potts model [80,81], which can be represented as correlated bond percolation by the Kasteleyn-Fortuin transformation, bond percolation and the Ising model correspond to the special cases with $q \to 1$ and $q = 2$, respectively. We also employ the isoradial mapping to derive an effective shear transformation [53] to relate the anisotropic Potts model to the isotropic Potts model for any real value $1 \leq q \leq 4$. The validity is supported by the consistent theoretical and numerical results for wrapping probability $R_2$ in Table S4 of the Supplemental Material [53]. This considerably extends the results for the Ising model which were obtained by a method combining anisotropic $\phi^4$ theory and exact correlation functions of the Ising model [75–77].

In short, we have shown that a nontrivial transformation relates anisotropic to isotropic percolation and Potts systems. The anisotropy can arise from the emergent phase, from the shape of constituent particles, or from anisotropic bond-placing rules. Our study is related to but different from previous investigations about the dependence of critical dimensionless quantities on the shape or boundary conditions of the overall system [51,52,67,69]. We anticipate that the transformation is valid for other boundary conditions, in higher dimensions and continuum space [33], and for anisotropy induced by other mechanisms [82], as long as correlations are weakly anisotropic [76]. The method of numerically determining $\rho_e$ from a known dimensionless quantity or exactly deriving shear parameters from isoradial graphs could be very useful for future research. Our Letter can have practical applications in other equilibrium and nonequilibrium phase transitions. For example, for the nematic transition of rods, variations of the Binder parameter were found but not well understood [83,84]. For

strongly anisotropic systems [85,86] with distinct correlation-length exponents, $\nu_{\parallel}$ and $\nu_{\perp}$, in the parallel and perpendicular directions, by carefully adopting a size-dependent rescaling factor $\propto L^{\nu_{\parallel}/\nu_{\perp}-1}$, the dimensionless quantities can be used as a powerful tool in locating phase transitions [87–90].

This work was supported by the National Natural Science Foundation of China under Grants No. 11905001 (H. H.) and No. 12275263 (Y. D.), and by the Anhui Provincial Natural Science Foundation under Grant No. 1908085QA23 (H. H.). We acknowledge the High-Performance Computing Platform of Anhui University for providing computing resources.

*huhao@ahu.edu.cn

[1] C. Casagrande and M. Veyssié, C. R. Acad. Sci. (Paris) **II-306**, 1423 (1988).
[2] P. G. de Gennes, Rev. Mod. Phys. **64**, 645 (1992).
[3] J. Lahann, Small **7**, 1149 (2011).
[4] J. Zhang, B. A. Grzybowski, and S. Granick, Langmuir **33**, 6964 (2017).
[5] A. Kirillova, C. Marschelke, and A. Synytska, ACS Appl. Mater. Interfaces **11**, 9643 (2019).
[6] X. Zhang, Q. Fu, H. Duan, J. Song, and H. Yang, ACS Nano **15**, 6147 (2021).
[7] F. Sciortino, A. Giacometti, and G. Pastore, Phys. Rev. Lett. **103**, 237801 (2009).
[8] Y. Iwashita and Y. Kimura, Soft Matter **9**, 10694 (2013).
[9] Q. Chen, S. C. Bae, and S. Granick, Nature (London) **469**, 381 (2011).
[10] X. Mao, Q. Chen, and S. Granick, Nat. Mater. **12**, 217 (2013).
[11] F. Sciortino, A. Giacometti, and G. Pastore, Phys. Chem. Chem. Phys. **12**, 11869 (2010).
[12] T. Vissers, Z. Preisler, F. Smallenburg, M. Dijkstra, and F. Sciortino, J. Chem. Phys. **138**, 164505 (2013).
[13] Z. Preisler, T. Vissers, F. Smallenburg, G. Munaò, and F. Sciortino, J. Phys. Chem. B **117**, 9540 (2013).
[14] D. J. Beltran-Villegas, B. A. Schultz, N. H. Nguyen, S. C. Glotzer, and R. G. Larson, Soft Matter **10**, 4593 (2014).
[15] Z. Preisler, T. Vissers, G. Munaò, F. Smallenburg, and F. Sciortino, Soft Matter **10**, 5121 (2014).
[16] Y. Iwashita and Y. Kimura, Soft Matter **13**, 4997 (2017).
[17] Y. Liang, B. Ma, and M. Olvera de la Cruz, Phys. Rev. E **103**, 062607 (2021).
[18] H. Shin and K. S. Schweizer, Soft Matter **10**, 262 (2014).
[19] Y. Iwashita and Y. Kimura, Soft Matter **10**, 7170 (2014).
[20] S. Jiang, J. Yan, J. K. Whitmer, S. M. Anthony, E. Luijten, and S. Granick, Phys. Rev. Lett. **112**, 218301 (2014).
[21] H. Rezvantalab, D. J. Beltran-Villegas, and R. G. Larson, Phys. Rev. Lett. **117**, 128001 (2016).
[22] Y. Iwashita and Y. Kimura, Sci. Rep. **6**, 27599 (2016).
[23] K. Mitsumoto and H. Yoshino, Soft Matter **14**, 3919 (2018).
[24] Z. Huang, G. Zhu, P. Chen, C. Hou, and L. T. Yan, Phys. Rev. Lett. **122**, 198002 (2019).
[25] T. Huang, Y. Han, and Y. Chen, Soft Matter **16**, 3015 (2020).
[26] I. Balberg, Phys. Rev. Lett. **119**, 080601 (2017).
[27] H. Tsurusawa, M. Leocmach, J. Russo, and H. Tanaka, Sci. Adv. **5**, eaav6090 (2019).
[28] J. H. Cho, R. Cerbino, and I. Bischofberger, Phys. Rev. Lett. **124**, 088005 (2020).
[29] L. Falsi, M. Aversa, F. Di Mei, D. Pierangeli, F. Xin, A. J. Agranat, and E. DelRe, Phys. Rev. Lett. **126**, 037601 (2021).
[30] D. Stauffer, *Introduction to Percolation Theory*, 2nd ed. (Taylor & Francis, London, 1992).
[31] M. Sahimi, *Applications of Percolation Theory* (Taylor & Francis, London, 1994).
[32] Q. Wang, Z. He, J. Wang, and H. Hu, Phys. Rev. E **105**, 034118 (2022).
[33] S. P. Finner, T. Schilling, and P. van der Schoot, Phys. Rev. Lett. **122**, 097801 (2019).
[34] S. P. Finner, A. Atashpendar, T. Schilling, and P. van der Schoot, Phys. Rev. E **100**, 062129 (2019).
[35] N. Araújo, P. Grassberger, B. Kahng, K. J. Schrenk, and R. M. Ziff, Eur. Phys. J. Spec. Top. **223**, 2307 (2014).
[36] A. A. Saberi, Phys. Rep. **578**, 1 (2015).
[37] A. Pelissetto and E. Vicari, Phys. Rep. **368**, 549 (2002).
[38] M. F. Sykes and J. W. Essam, Phys. Rev. Lett. **10**, 3 (1963).
[39] M. F. Sykes and J. W. Essam, J. Math. Phys. (N.Y.) **5**, 1117 (1964).
[40] I. Balberg and N. Binenbaum, Phys. Rev. A **31**, 1222(R) (1985).
[41] R. Kenyon, *School and Conference on Probability Theory*, Lecture Notes Series Vol. 17 (ICTP, Trieste, 2004), pp. 268–304.
[42] G. R. Grimmett and I. Manolescu, Probab. Theory Related Fields **159**, 273 (2014).
[43] Y. Y. Tarasevich, N. I. Lebovka, and V. V. Laptev, Phys. Rev. E **86**, 061116 (2012).
[44] P. Longone, P. M. Centres, and A. J. Ramirez-Pastor, Phys. Rev. E **85**, 011108 (2012).
[45] P. Longone, P. M. Centres, and A. J. Ramirez-Pastor, Phys. Rev. E **100**, 052104 (2019).
[46] A. Patrykiejew and W. Rżysko, Physica (Amsterdam) **570A**, 125819 (2021).
[47] A. Patrykiejew and W. Rżysko, Soft Matter **16**, 6633 (2020).
[48] N. Kern and D. Frenkel, J. Chem. Phys. **118**, 9882 (2003).
[49] H. Hu and Y. Deng, Nucl. Phys. **B898**, 157 (2015).
[50] P. di Francesco, H. Saleur, and J. B. Zuber, J. Stat. Phys. **49**, 57 (1987).
[51] H. T. Pinson, J. Stat. Phys. **75**, 1167 (1994).
[52] R. M. Ziff, C. D. Lorenz, and P. Kleban, Physica (Amsterdam) **266A**, 17 (1999).
[53] See Supplemental Material at http://link.aps.org/supplemental/10.1103/PhysRevLett.129.278002 for: (1) Details for the system of close-packed Janus disks, including those for the thermodynamic phase transition and those for the percolation transition. (2) Details for the system of aligned rigid rods. (3) Details for anisotropic bond percolation, which verify the theoretical results obtained using the method of isoradial graphs. The shear parameters for the honeycomb lattice are also given by using the star-triangle transformation. (4) A script for calculating exact values of wrapping probabilities for standard percolation in 2D using

expressions from the literature. (5) Preliminary results for anisotropic $q$-state Potts model on the triangular lattice.
[54] H. Duminil-Copin, J.-H. Li, and I. Manolescu, Electron. J. Probab. **23**, 1 (2018).
[55] C. Zamora-Ledezma, C. Blanc, N. Puech, M. Maugey, C. Zakri, E. Anglaret, and P. Poulin, Phys. Rev. E **84**, 062701 (2011).
[56] T. Ackermann, R. Neuhaus, and S. Roth, Sci. Rep. **6**, 34289 (2016).
[57] K. Thorkelsson, P. Bai, and T. Xu, Nano Today **10**, 48 (2015).
[58] S. Jiang and S. Granick, Langmuir **24**, 2438 (2008).
[59] C. R. Scullard and R. M. Ziff, Phys. Rev. Lett. **100**, 185701 (2008).
[60] C. R. Scullard and R. M. Ziff, J. Stat. Mech. (2010) P03021.
[61] C. R. Scullard, J. Stat. Mech. (2011) P09022.
[62] C. R. Scullard and J. L. Jacobsen, J. Phys. A **45**, 494004 (2012).
[63] S. Mertens and R. M. Ziff, Phys. Rev. E **94**, 062152 (2016).
[64] C. R. Scullard and J. L. Jacobsen, Phys. Rev. Res. **2**, 012050(R) (2020).
[65] W. Xu, J. Wang, H. Hu, and Y. Deng, Phys. Rev. E **103**, 022127 (2021).
[66] J. L. Jacobsen and C. R. Scullard, J. Phys. A **46**, 075001 (2013).
[67] R. P. Langlands, C. Pichet, Ph. Pouliot, and Y. Saint-Aubin, J. Stat. Phys. **67**, 553 (1992).
[68] G. Kamieniarz and H. W. J. Blöte, J. Phys. A **26**, 201 (1993).
[69] A. Malakis, N. G. Fytas, and G. Gülpinar, Phys. Rev. E **89**, 042103 (2014).
[70] X. S. Chen and V. Dohm, Phys. Rev. E **70**, 056136 (2004).
[71] W. Selke and L. N. Shchur, J. Phys. A **38**, L739 (2005).
[72] W. Selke and L. N. Shchur, Phys. Rev. E **80**, 042104 (2009).
[73] B. Kastening, Phys. Rev. E **87**, 044101 (2013).
[74] H. Hobrecht and A. Hucht, SciPost Phys. **7**, 26 (2019).
[75] V. Dohm, Phys. Rev. E **100**, 050101(R) (2019).
[76] V. Dohm and S. Wessel, Phys. Rev. Lett. **126**, 060601 (2021).
[77] V. Dohm, S. Wessel, B. Kalthoff, and W. Selke, J. Phys. A **54**, 23LT01 (2021).
[78] Y. Deng and H. W. J. Blöte, arXiv:cond-mat/0508348.
[79] H. Hu, H. W. Blöte, and Y. Deng, J. Phys. A **45**, 494006 (2012).
[80] F. Y. Wu, Rev. Mod. Phys. **54**, 235 (1982).
[81] L. P. Arguin, J. Stat. Phys. **109**, 301 (2002).
[82] R. H. J. Otten and P. van der Schoot, Phys. Rev. Lett. **108**, 088301 (2012).
[83] L. G. López, D. H. Linares, A. J. Ramirez-Pastor, and S. A. Cannas, J. Chem. Phys. **133**, 134706 (2010).
[84] N. G. Almarza, J. M. Tavares, and M. M. Telo da Gama, J. Chem. Phys. **134**, 071101 (2011).
[85] M. Henkel, Nucl. Phys. **B641**, 405 (2002).
[86] N. Kyriakopoulos, H. Chaté, and F. Ginelli, Phys. Rev. E **100**, 022606 (2019).
[87] K. Binder, in *Finite Size Scaling and Numerical Simulations of Statistical Systems*, edited by V. Privman (World Scientific, Singapore, 1990), Chap. 4, p. 174.
[88] D. Winter, P. Virnau, J. Horbach, and K. Binder, Europhys. Lett. **91**, 60002 (2010).
[89] S. Angst, A. Hucht, and D. E. Wolf, Phys. Rev. E **85**, 051120 (2012).
[90] C. Norrenbrock, M. M. Mkrtchian, and A. K. Hartmann, Phys. Rev. E **100**, 022113 (2019).